Turbulent convective mass transfer downstream of a perforated baffle blockage

M. Molki and A. Hashemi-Esfahanian
Department of Mechanical Engineering, Esfahan University of Technology, Esfahan, Iran

An experimental investigation has been performed to determine convective heat transfer downstream of a perforated baffle blockage situated on the lower principal wall of a rectangular duct. The experiments were carried out via a mass transfer technique, which enabled a local measurement of transfer coefficients. The study was confined to blockage ratio $h/H = 0.5$, the Reynolds number ranged from 5,000–30,000, and the test duct had a 5:1 aspect ratio. The performance evaluation indicated that, under identical mass flow, the baffle plate improved the transfer coefficients, while under other constraints no improvement was observed.

Keywords: turbulent duct flow; convective mass transfer; perforated blockage; recirculating flow

Introduction

Turbulent heat transfer in flow passages with baffle blockages occurs in many engineering devices. The baffle plates either deflect the main stream and, thereby, create additional mixing in the flow, or provide more surface area for heat transfer. Both these features tend to augment convection from the hot surfaces.

The presence of the baffle is usually accompanied by a large pressure drop, which, under certain constraints, might offset the advantages gained through augmentation of heat transfer. It has been shown that when flow-obstruction techniques are employed to enhance heat transfer, the pressure drops are often so large that the use of the technique may only be justified through a careful evaluation of thermal-hydraulic performance of the flow field (Sparrow and Comb 1983, Molki and Mostoufizadeh 1989).

While a simple solid baffle plate attached to the duct wall enhances heat transfer, a perforated plate attached to the same duct wall poses less resistance to the flow and, thus, might have a better performance. The present investigation is focused on the thermal-hydraulic behavior of a single perforated baffle plate attached to one of the principal walls of a rectangular duct.

Apparently, no prior experimental work on the subject has appeared in the literature. There are, however, a number of works that are in some respects related to the present problem. For instance, wind tunnel studies for flow around solid baffles (Good and Joubert 1968), the effect of a sudden step change in wall profile on turbulent flow in heated ducts (Baughn *et al.* 1984, Vogel and Eaton 1985, Garcia and Sparrow 1987), and the flow through ducts with baffle blockages (Berner *et al.* 1984, Webb and Ramadhyani 1985, Kelkar and Patankar 1987) have all been addressed before.

The experiments of the present investigation were carried out in a rectangular duct, with a single baffle plate situated on the lower principal wall. We wanted to have a duct where a certain length of the lower wall, downstream from the baffle plate, was thermally active and participated in heat transfer, while the other walls and the baffle plate itself were all adiabatic. In this regard, a mass transfer procedure (naphthalene sublimation) was employed to achieve the desired boundary conditions, and the well-known analogy between heat and mass transfer (Eckert 1976) provided the link between the two processes.

The local mass measurements were performed for three different cases, namely, the smooth duct, duct with the solid baffle, and duct with the perforated baffle. In experiments with baffle plates, the blockage ratio h/H was equal to 0.5. The Reynolds number ranged from 5,000–30,000, and the mass transfer measurements were carried out at 10 axial stations and extended six hydraulic diameters downstream.

In another part of the research, the flow field was visualized by means of the oil-lampblack technique. Moreover, the pressure drop across the test section was measured, and the results were combined with mass transfer data to evaluate the optimal performance.

Experimental apparatus and procedure

The schematic view of the experimental setup is shown in Figure 1a. The apparatus consists of a straight rectangular duct having cross-sectional dimensions of $W = 10 \pm 0.02$ cm by $H = 2 \pm 0.02$ cm, with a hydraulic diameter $D_h = 3.33 \pm 0.028$ cm and a 5:1 aspect ratio. As seen, the rectangular duct is made of three parts: a hydrodynamic development length ($33D_h$), the test section ($6D_h$), and a post-test section length ($12D_h$). Other important elements on the flow circuit are a calibrated orifice plate, with a coefficient $C_D = 0.5976 \pm 0.0226$, a control valve, and a centrifugal fan, which operated in the suction mode.

Figure 1b shows the schematic of the test section. The lower wall (length L × width $W = 20 \times 10$ cm) was removable and was coated with a layer (about 0.7 cm thick) of solid naphthalene ($C_{10}H_8$) through casting. To facilitate the flow visualization experiments, the upper wall of the test section was made of Plexiglas.

The baffle plates were made of sheet metal having a thickness

Address reprint requests to Dr. Molki at the Department of Mechanical Engineering, Esfahan University of Technology, Esfahan, Iran.

Received 26 February 1991; accepted 26 November 1991

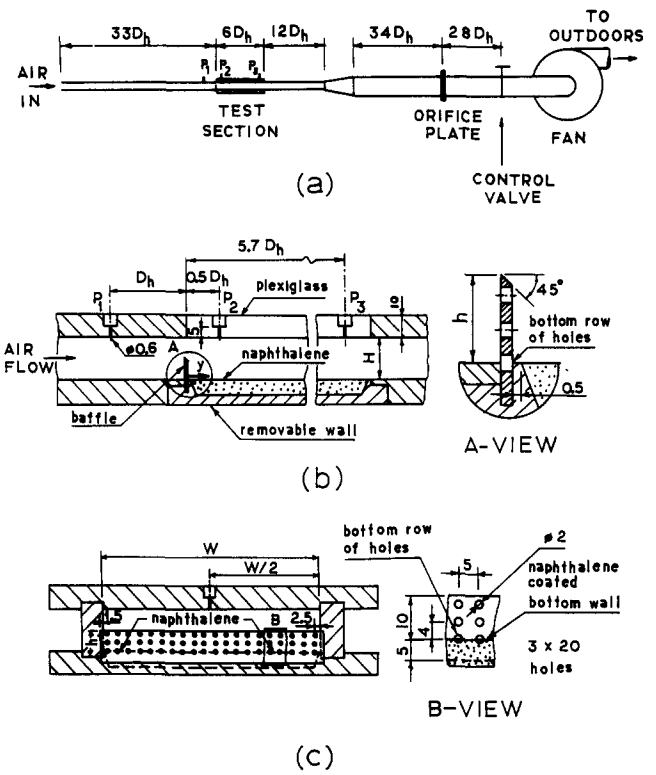

Figure 1 The experimental apparatus (all dimensions in millimeters)

of 0.15 cm, with a height $h = 1$ cm. The baffle plates were either solid or perforated. The orientation of the perforated baffle is shown in Figures 1b and c. The perforated plate was formed by drilling 3 x 20 circular holes through the plate arranged in lines. The diameter of each hole was 0.2 cm.

The local mass measurements were made on a coordinate table that could be traversed along two horizontal coordinates, namely, x and y. The origin of the coordinate system was at the intersection of the longitudinal axis of the naphthalene surface and the baffle plate, with y situated along the direction of main flow (Figure 1b) and x perpendicular to it. The horizontal traverse of the coordinate table in the x- and y-directions could be measured with an accuracy of ± 0.1 mm.

During the run, these variables were recorded: temperature (± 0.2°C), duration of the run (± 1 s), barometric pressure (± 1 mm Hg), and air pressures (three at the test section and two at orifice plate, ± 1 mm H_2O). Immediately before and after each run, the test section wall was placed on the coordinate table and the surface elevations were measured (± 0.001 mm) at 50 equally spaced points.

To visualize the flow field, a suitable mixture of engine oil and fine lampblack powder was applied to the test section wall. When airflow was initiated, the black oily mixture moved under the action of shear stress exerted by the air, and the streaks that formed on the surface revealed the pattern of flow field adjacent to the wall. The photographic evidence of the flow visualizations is presented and discussed later in this paper.

Data reduction

Local mass transfer coefficients, $K(x, y)$, were calculated from

$$K(x, y) = m(x, y)/[\rho_{nw} - \rho_{nb}(y)] \quad (1)$$

Notation

A_t	Area of the orifice, Equation 10
C_B	Discharge coefficient in Equation 11
C_D	Discharge coefficient of the orifice, Equation 10
D_h	Hydraulic diameter, $2WH/(W + H)$
f	Friction factor, Equation 12
H	Duct height, Figure 1b
h	Plate height, Figure 1b, heat transfer coefficient in Nu
K	Mass transfer coefficient, Equation 1, loss coefficient $(L/D_h)f$
$\bar{K}$	Average mass transfer coefficient, Equation 5
k	Thermal conductivity in Nu
L	Streamwise length of naphthalene-coated wall
LMDD	Logarithmic mean density difference, Equation 7
M	Average rate of mass transfer per unit area, Equation 6
m	Local rate of mass transfer per unit area, Equation 2
Nu	Nusselt number, hD_h/k
P_1	Air pressure at $1D_h$ upstream of plate location, Figure 1
P_2	Air pressure at $0.5D_h$ downstream of plate location, Figure 1
ΔP	Pressure difference across the test section, $P_1 - P_3$
Q	Volumetric air flow rate, Equation 10
Re	Reynolds number, Equation 9
Re*	Modified Reynolds number, 0.832Re (Jones, 1976)
Sc	Schmidt number, Equation 4
Sh	Sherwood number, Equation 4
$\overline{\text{Sh}}$	Average Sherwood number, Equation 8
t	Duration time of data run, Equation 2
$u_{(\ )}$	Relative uncertainty of the quantity ( )
V	Mean air velocity, Equation 9
W	Duct width, Equation 9
w	Mass flow rate of air, Equation 10
w_i	Mass flow rate of air through plate perforations, Equation 11
x	Transverse coordinate, Equation 1
y	Streamwise coordinate, Figure 1b
y_{max}	y at the point of maximum transfer coefficient

Greek symbols

β	Ratio of orifice diameter to pipe diameter, Equation 10
δ	Local change in elevation of naphthalene surface due to sublimation, Equation 2
δ_{av}	Average δ, Equation 3
ν	Kinematic viscosity, Equation 4
ρ	Density, Equation 12
ρ_{nb}	Naphthalene vapor density in bulk, Equation 1
ρ_{nw}	Naphthalene vapor density at wall, Equation 1
ρ_s	Density of solid naphthalene, Equation 2
ρ_{ts}	Air density, Equation 11

Subscripts

b	Baffle, Equations 20–22
max	Maximum value, Equations 13 and 14
pb	Perforated baffle, Figure 7
sb	Solid baffle, Figure 6

where $m(x, y)$ is the rate of mass transfer per unit area at point (x, y), and ρ_{nw} and $\rho_{nb}(y)$ denote, respectively, the wall and bulk values of naphthalene vapor density.

The value of $m(x, y)$ is evaluated from

$$m(x, y) = \rho_s \delta(x, y)/t \tag{2}$$

where ρ_s is the density of solid naphthalene (specific gravity = 1.145 referred to water at 4°C; Perry and Green 1987), $\delta(x, y)$ is the difference in elevation measurements at (x, y), and t is the duration of the run.

To determine ρ_{nw}, the naphthalene vapor pressure was evaluated from Sogin's (1958) vapor pressure–temperature correlation and the ideal gas equation. It should be noted that the test section was isothermal and, therefore, ρ_{nw} was the same for the entire naphthalene surface.

Next, at a fixed axial station y, the $\delta(x, y)$s were averaged with respect to x. The average values, $\delta_{av}(y)$, were then used to calculate $\rho_{nb}(y)$ from

$$\rho_{nb}(y) = (\rho_s W/tQ) \int_0^y \delta_{av}(y)\, dy \tag{3}$$

In Equation 3, the volume flow rate, Q, was calculated at the mean pressure of the test section.

Then, the local mass transfer coefficients were expressed as Sherwood numbers.

$$\mathrm{Sh}(x, y) = K(x, y) D_h \mathrm{Sc}/\nu \tag{4}$$

In Equation 4, the hydraulic diameter is $D_h = 2WH/(W + H)$, the Schmidt number for diffusion of naphthalene into air is Sc = 2.5, and the kinematic viscosity, ν, was taken as that for pure air.

The average mass transfer coefficient, $\bar{K}(y)$, for the length of duct between $y = 0$ and $y = y$ was determined from

$$\bar{K}(y) = M(y)(\mathrm{LMDD}) \tag{5}$$

where

$$M(y) = (1/Wy) \int_{y=0}^{y} \int_{x=-W/2}^{W/2} m(x, y)\, dx\, dy \tag{6}$$

In Equation 5, the logarithmic mean density difference, LMDD, is defined as

$$\mathrm{LMDD} = \rho_{nb}(y)/\ln\{\rho_{nw}/(\rho_{nw} - \rho_{nb}(y))\} \tag{7}$$

Then, the average coefficients were expressed in terms of Sherwood number.

$$\overline{\mathrm{Sh}}(y) = \bar{K}(y) D_h \mathrm{Sc}/\nu \tag{8}$$

The mass (heat) transfer results will be presented in terms of Reynolds number, Re, defined as

$$\mathrm{Re} = V D_h/\nu = 2w/\mu(H + W) \tag{9}$$

The mass flow rate of air, w, through the duct was evaluated from the orifice formula

$$w = \rho Q = C_D A_t [2\rho \Delta P/(1 - \beta^4)]^{0.5} \tag{10}$$

in which A_t is the area of the orifice ($= 6.158 \times 10^{-4}$ m^2) and β (the ratio of the orifice diameter to the pipe diameter) is equal to 0.7.

Another relevant parameter in the present investigation is the fluid injection ratio, w_i/w, for the perforated baffle plate. To find w_i/w, the free flow area between the plate edge and the opposite principal wall was treated as an orifice plate and was calibrated in terms of pressure drop across the baffle plate. Thus,

$$w_i/w = 1 - C_B[\rho_{ts}(P_1 - P_2)]^{0.5}/w \tag{11}$$

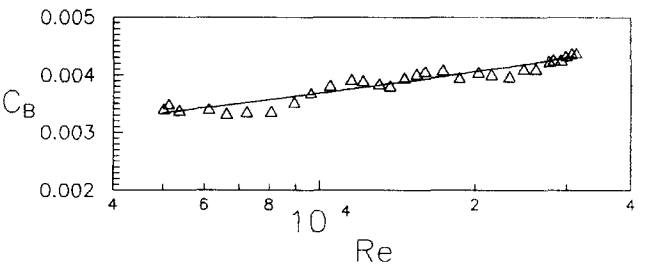

Figure 2 Distribution of C_B *versus* Re

The coefficient C_B is presented in Figure 2. The mean C_B, based on 30 data points, is 3.886×10^{-3}. The solid line seen in the figure is the least-squares fit through the data with equation $C_B = 0.00101\mathrm{Re}^{0.141}$.

The pressure measurements across the test section were employed to evaluate the friction factor, f, as

$$f = D_h(\Delta P/L)/(0.5\rho V^2) \tag{12}$$

In Equation 12, ΔP is the pressure drop across the test section.

The experimental uncertainties were also evaluated. If the uncertainty of independent quantities are temperature, ±0.2°C; time, ±1 s; barometric pressure, ±1 mm Hg; air pressures, ±1 mm H_2O; elevation measurement, ±0.001 mm; discharge coefficient of the orifice, ±0.0226; and the duct hydraulic diameter, ±0.028 cm, then, for a typical run at Re = 16,500, we obtain the following relative uncertainties (Kline 1985, Abernethy *et al.* 1985):

$$u_{\mathrm{Re}} = \pm 3.8\%, \quad u_{\mathrm{Sh}} = \pm 2.5\%, \quad u_{\overline{\mathrm{Sh}}} = \pm 2.7\%, \quad u_f = \pm 12.5\%$$

Results and discussion

The results are presented in three parts: (1) the flow visualization, (2) the mass (heat) transfer, and (3) the performance. First, attention is turned to flow visualization.

Flow visualization

The photographic evidence of the flow field is shown in Figure 3. These photographs show the top view of the flow patterns near the lower principal wall of the test section. The scale below each figure indicates the distance from the baffle plate in centimeters, with $y = 0$ corresponding to the location of the plate. The main airflow is from left to right.

Figure 3a corresponds to the flow downstream of the solid baffle plate. As is expected, there is a recirculating zone in this region that extends from about $y = 3$–11 cm; between $y = 3$ and 11 cm, there is a backflow near the wall and the air moves upstream. The relatively dark, thick line at $y = 11$ cm is the line of flow reattachment. Further downstream, the airflow is along the direction of the main flow.

Good and Joubert (1968) have also predicted a similar location for flow reattachment. Their experiments were carried out in a wind tunnel with a 4-inch (10.16 cm) vertical flat plate attached to the lower wall of tunnel. They indicated that the flow reattachment occurred at $y/h = 13.3$, while Figure 3a gives $y/h = 11$. The slightly earlier occurrence of flow reattachment in the present study is seemingly due to the resistance imposed by the duct walls.

In the region from $y = 0$ to about 3 cm, there is another recirculating zone. In this region, the air near the downstream face of the baffle plate moves downward, and then adjacent to the wall it moves downstream from $y = 0$–3 cm. The

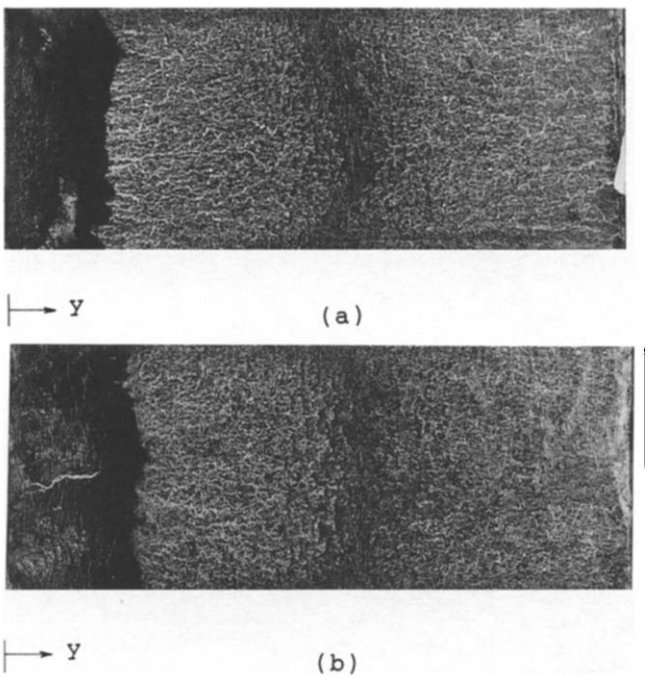

Figure 3 Photographs of flow visualization. (a) Solid baffle; (b) perforated baffle

recirculating motion of air in this vortex is rather weak and is hardly able to move the black mixture.

Another noteworthy feature in Figure 3a is the curvature of reattachment line, which is the evidence of three dimensionality of the flow field. While the flow between infinitely wide parallel plates are two dimensional, the interaction between the duct side walls and the flow downstream of the plate has created a three-dimensional situation.

Figure 3b presents the flow patterns for the perforated baffle plate. The overall view of the flow pattern is almost similar to that of Figure 3a. It is seen that the line of flow reattachment has slightly moved downstream and occurs at about $y = 11.5$ cm. Moreover, the three dimensionality of the flow field is less noticeable. Furthermore, the near plate corner vortex of Figure 3a is now replaced by the more active jet flows emerging from the perforated baffle.

Mass (heat) transfer results

The local mass transfer coefficients, $\mathrm{Sh}(x, y)$, for the smooth duct at $\mathrm{Re} = 30{,}000$ are shown in Figure 4. Comparison of $\mathrm{Sh}(x, y)$ at symmetric values of transverse coordinate x ($x = 0$ is on the lower wall and situated midway between the side walls) indicates symmetry about the duct axis. However, there are some variations of $\mathrm{Sh}(x, y)$ along the x-axis.

The $\mathrm{Sh}(x, y)$s were subsequently averaged with respect to x and the averages, which are indicated by $\mathrm{Sh}(y)$ (or $\mathrm{Nu}(y)$), are presented in Figure 5 (the Sh–Nu conversion has been explained briefly by Molki *et al.* 1990). It is seen that close to $y = 0$, where the mass concentration (or thermal) boundary layer is thin, the transfer coefficients are very large. Further downstream, the boundary layer grows and the coefficients decrease.

In this figure, the results of present study are compared with those of other investigators. Incropera *et al.* (1986) obtained their averaged results for square heating elements through a direct heat transfer method, while those of Sparrow *et al.* (1987) are semi-local mass transfer coefficients. Although the experimental details of these studies are somewhat different, the figure indicates a relatively good agreement among them.

The local transfer coefficients downstream of the solid baffle plate ($w_i/w = 0$) are presented in Figure 6. The rather small value of transfer coefficients near the baffle, the peak value, and the subsequent decrease of coefficients are all indicative of flow separation, followed by a reattachment and redevelopment.

The point of maximum Sherwood number at $\mathrm{Re} = 30{,}000$

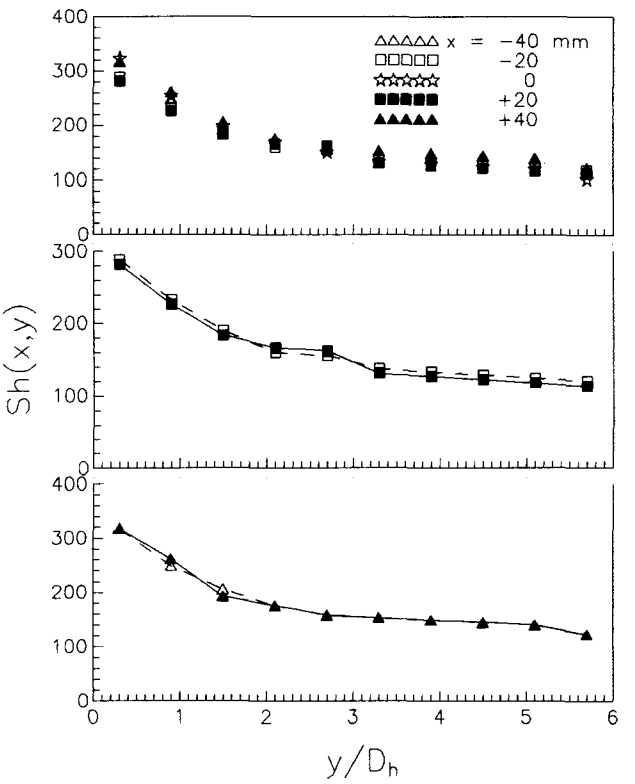

Figure 4 A typical distribution of local Sherwood number at five different transverse locations for the smooth duct. Re = 30,000

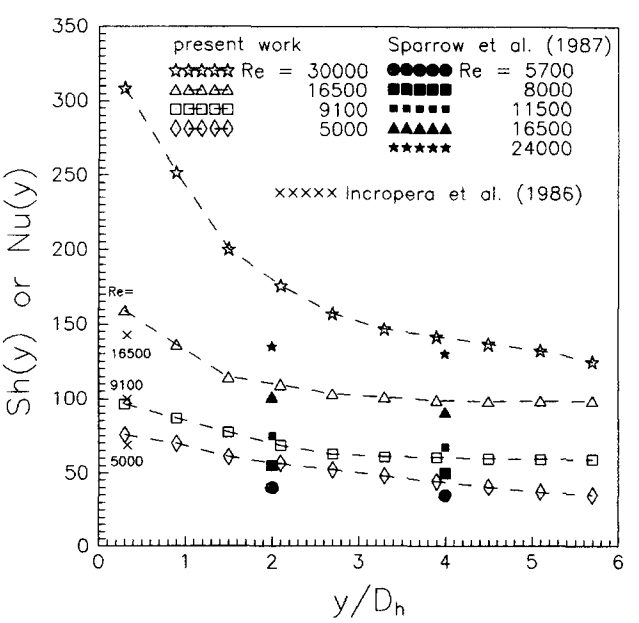

Figure 5 Distribution of transfer coefficients for the smooth duct and comparison with literature

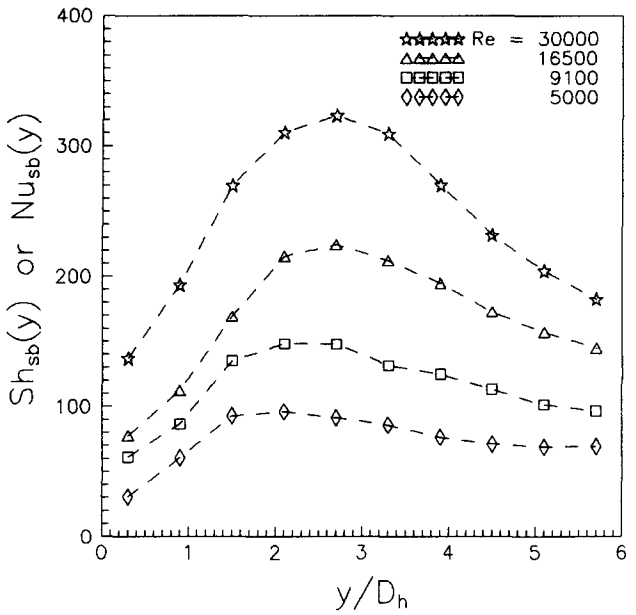

Figure 6 Distribution of transfer coefficients for the duct with solid baffle. $w_i/w = 0$

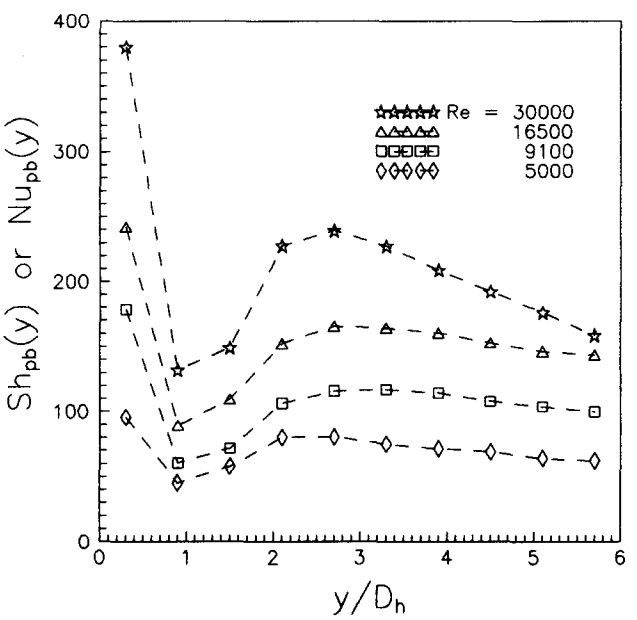

Figure 7 Distribution of transfer coefficients for the duct with perforated baffle. $w_i/w = 0.264$

(corresponding to Re of flow visualization experiments) is at $y_{max} = 9.0$ cm (i.e., $y_{max}/D_h = 2.7$) and occurs before the point of reattachment. It has been shown (Vogel and Eaton 1985) that the location of maximum heat transfer for the separated flow downstream of a backward-facing step is 0.9 of y at the point of reattachment, which is comparable to the value (9.0/11 =) 0.82 in the present study.

Mass (heat) transfer coefficients downstream of the perforated baffle ($w_i/w = 0.264$) are given in Figure 7. Starting with a relatively high value near the baffle plate, the Sherwood number decreases rapidly to a minimum, whereupon it experiences a systematic increase and decrease similar to the trend observed in Figure 6.

As is evident from flow visualization photographs (Figure 3b), the effect of fluid jets emerging from the perforated plate extends downstream to $y = 3.5$ cm ($y/D_h = 1.05$) and, apparently, sweeps out the corner vortex. These highly active flow processes are reflected in the initial portion of the curves of Figure 7.

Also, the spanwise profiles of Sh for the perforated baffle are shown in Figure 8. These profiles should somewhat clarify the true meaning of the averages presented in Figure 7.

The maximum Sherwood numbers (Figure 9) are correlated as

$$Sh_{max} = 0.300Re^{0.679} \quad \text{(solid baffle)} \tag{13}$$

$$Sh_{max} = 0.467Re^{0.605} \quad \text{(perforated baffle)} \tag{14}$$

The exponent 2/3, which well approximates the exponents 0.679 and 0.605 in Equations 13 and 14, is very common in turbulent separated and reattached flows. Also shown in this figure are the following experimental results: Garcia and Sparrow (1987), $0.357Re^{0.69}$; Mills (1962), $0.282Re^{0.683}$; and Krall and Sparrow (1966), $0.282Re^{2/3}$. Although the apparatus involved in these references have different separation-producing geometries, the agreement among the exponents of Re is remarkable.

Figure 10 compares the local values of Sh, Sh_{sb}, and Sh_{pb}. The figure indicates that, except for the first few data, the presence of baffle (solid or perforated) has increased the local transfer coefficients to values higher than those of the smooth duct. However, at larger distances from the baffle, this increasing effect diminishes and the ratio of Sherwood numbers approaches unity.

The average Sherwood number, $\overline{Sh}$, for the entire naphthalene coated wall are plotted *versus* Re in Figure 11.

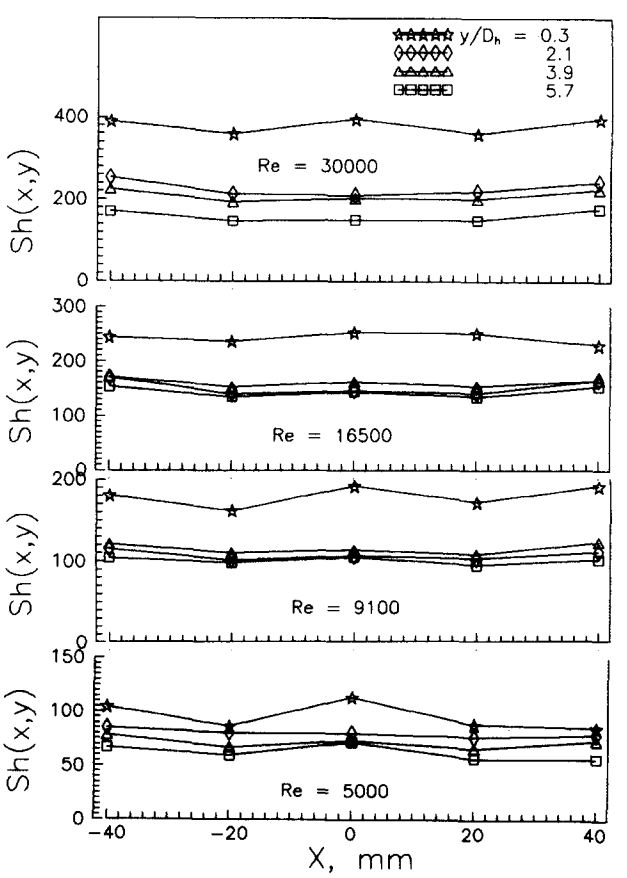

Figure 8 Spanwise distribution of Sh for the perforated baffle

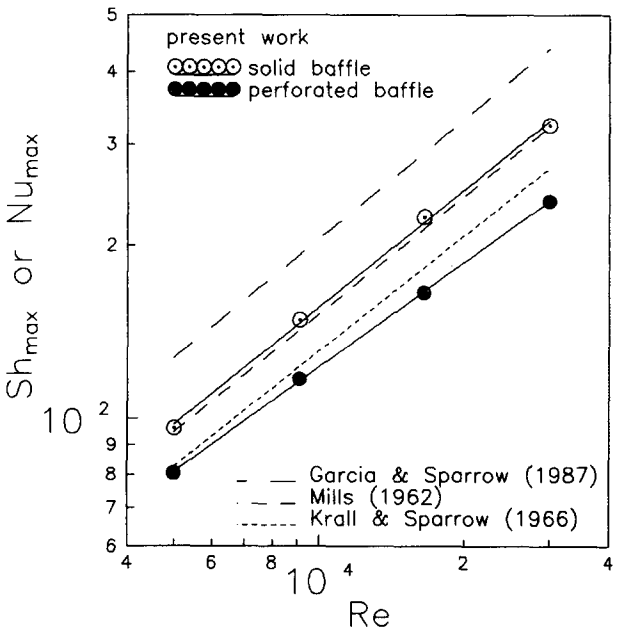

Figure 9 The maximum transfer coefficients downstream of the solid and perforated baffle

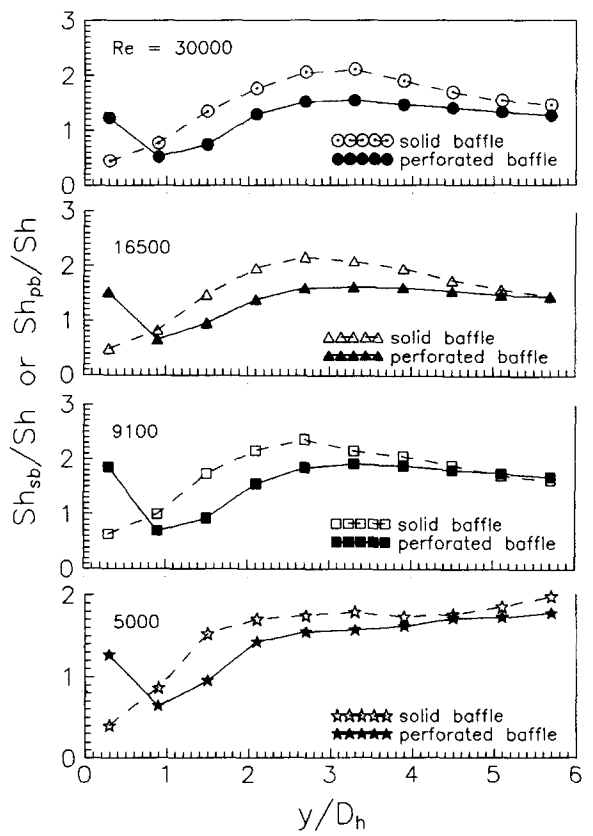

Figure 10 Comparison of local Sherwood numbers

The straight lines passing through the data are the least-squares fits with the equations

$$\overline{Sh} = 0.133Re^{0.696} \quad \text{(no baffle)} \tag{15}$$

$$\overline{Sh} = 0.265Re^{0.664} \quad \text{(solid baffle)} \tag{16}$$

$$\overline{Sh} = 0.398Re^{0.611} \quad \text{(perforated baffle)} \tag{17}$$

The air pressure (relative to atmosphere, P_{atm} = 615.3 mm Hg) and the corresponding friction factors are shown in Figures 12 and 13. Also plotted in Figure 13 is the Blasius equation, $f = 0.3164(Re^*)^{-0.25}$, where $Re^* = 0.832Re$ is the modified Reynolds number (Jones 1976). Comparison of the results indicates that the overall pressure drop is larger for the solid baffle. Using the least-squares method, the equations for f are

$$f = 21.339Re^{-0.415} \quad \text{(solid baffle)} \tag{18}$$

$$f = 13.940Re^{-0.395} \quad \text{(perforated baffle)} \tag{19}$$

where fs may readily be converted to Ks through $K = (L/D_h)f$.

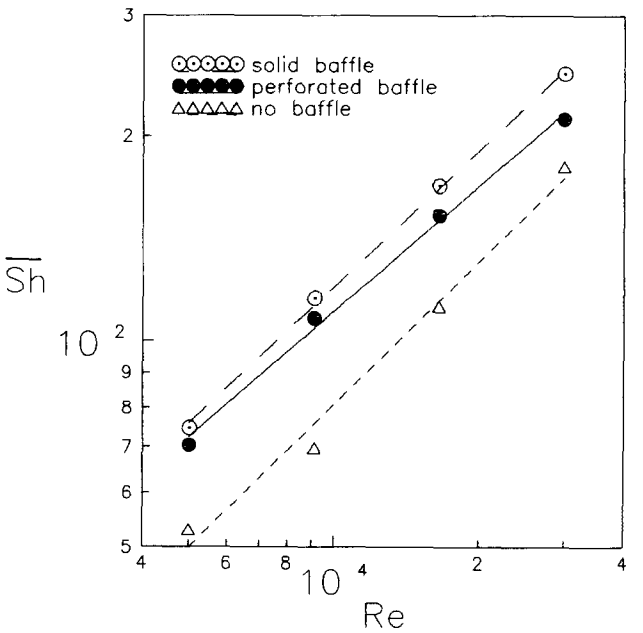

Figure 11 Average Sherwood number over a 20-cm length of duct wall

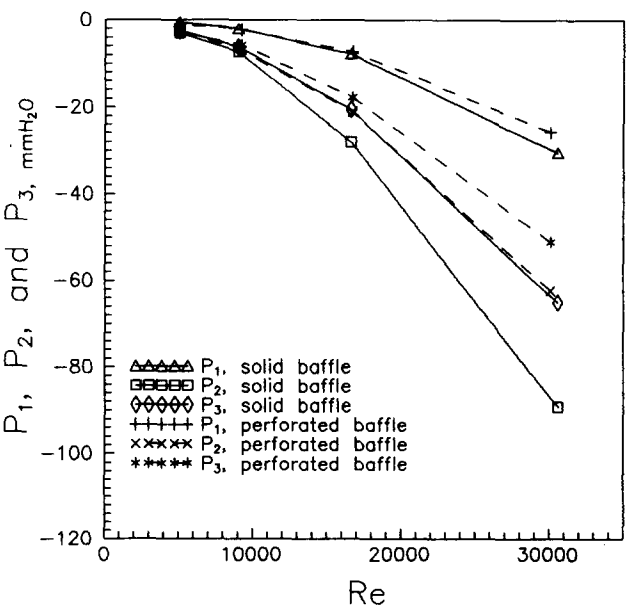

Figure 12 Pressure data for the solid and perforated baffle

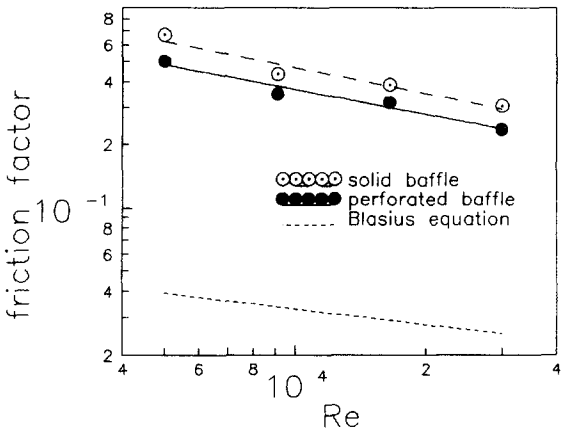

Figure 13 Friction factor, f

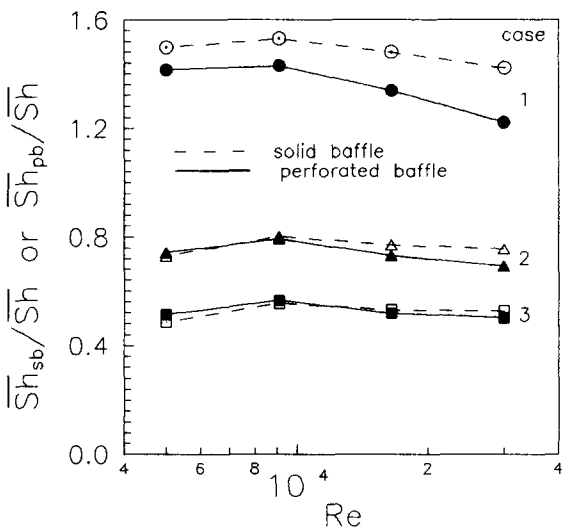

Figure 14 Performance evaluation

Performance evaluation

The thermal-hydraulic performance of the duct may be investigated in three different cases: (1) equal mass flow rate, (2) equal pumping power, and (3) equal pressure drop per unit length. These cases are expressed by the following constraints:

Case 1 $\mathrm{Re}_b = \mathrm{Re}$ (20)

Case 2 $(f\mathrm{Re}^3)_b = f\mathrm{Re}^3$ (21)

Case 3 $(f\mathrm{Re}^2)_b = f\mathrm{Re}^2$ (22)

In Equations 20–22, the subscript b identifies the duct with baffle blockage, and the no-subscript variables on the right are for the smooth (no-baffle) duct.

With the aid of Equations 18–22, together with Blasius equation for the smooth duct, to each selected Reynolds number for flow through the duct with baffle plate, there is a corresponding value of Re for the smooth duct. Therefore, the values of $\overline{Sh}$, $\overline{Sh}_{sb}$, and $\overline{Sh}_{pb}$ can be evaluated from Equations 15–17 at the respective Reynolds numbers. The ratios $\overline{Sh}_{sb}/\overline{Sh}$ and $\overline{Sh}_{pb}/\overline{Sh}$ are plotted in Figure 14.

It is seen in this figure that, for equal mass flow rates (case 1), the presence of a baffle plate enhances the transfer coefficients. In the range of Re considered in this study, the amount of enhancement for the solid and perforated baffle ranged, respectively, from 42–53 percent and 22–43 percent.

However, for other constraints, it is evident from Figure 14 that the presence of the baffle decreases the transfer coefficients. In this regard, the constraint corresponding to case 3 entails the largest decrease in Sherwood number. The value of ($\overline{Sh}_{sb}/\overline{Sh}$ and $\overline{Sh}_{pb}/\overline{Sh}$) for case 2 and case 3 range, respectively, from (0.73–0.80 and 0.69–0.79) to (0.49–0.56 and 0.50–0.57). These values correspond to a reduction of (27–20 percent and 31–21 percent) to (51–44 percent and 50–43 percent) in the average Sherwood numbers. Further, it is noteworthy that the presence of perforations on the baffle plate does not have a significant effect on $\overline{Sh}$ ratios.

Using the results of Sparrow and Wachtler (1978) and those of the present study, it may be shown that, for Re = 5,000–30,000, the average Sherwood number for the combination of nonadiabatic baffle plate plus the lower duct wall is, on the average, 3.6 percent higher than those of the lower wall alone. The single nonadiabatic plate also increases the transfer surface area by 10 percent. Therefore, it is evident that the 10 + 3.6 percent = 13.6 percent increase in mass transfer due to the plate fin effect is not sufficiently large to compensate the aforementioned reductions in Sherwood numbers.

Concluding remarks

This study has revealed the local transfer characteristics of turbulent flow downstream of a wall-attached solid or perforated baffle plate in a rectangular duct. For the experiments, the Reynolds number ranged from 5,000–30,000, while the blockage ratio, h/H, was fixed at 0.5.

The flow visualization indicated a large recirculating zone downstream from the plate. The flow reattachment occurred at $y = 11h$ and the slightly curved reattachment line pointed to the three dimensionality of the flow field. A small vortex was also recognized in the downstream corner of baffle plate.

In the case of perforated plate, the line of reattachment slightly moved downstream and occurred at about $y = 11.5h$. Moreover, the corner vortex of solid plate was replaced by the more active jet flows emerging from the perforated plate.

The peak transfer coefficient in the flow separation zone downstream of the solid baffle occurred earlier than reattachment and was located at $y_{max} = 9.0$ cm. This peak coefficient was also observed in the experimental results of perforated plate.

Finally, the mass (heat) transfer and pressure drop data were combined to evaluate the performance of the duct. In the range of parameters employed in this study, the perforated plate did not show any thermal advantage over the solid plate.

Acknowledgment

The authors gratefully acknowledge a grant from the Research Council of Esfahan University of Technology. We are also grateful to H. Gafar-Pisheh and Haj-Naseri for fabricating a part of the experimental apparatus.

References

Abernethy, R. B., Benedict, R. P. and Dowdell, R. B. 1985. ASME measurement uncertainty. *J. Fluids Eng.* **107**, 161–164

Baughn, J. W., Hoffman, M. A., Takahashi, R. K. and Launder, B. E. 1984. Local heat transfer downstream of an abrupt expansion in a circular channel with constant wall heat flux. *ASME J. Heat Transfer* **106**, 789–796

Berner, C., Durst, F. and McEligot, D. M. 1984. Flow around baffles. *ASME J. Heat Transfer* **106**, 743–749

Eckert, E. R. G. 1976. Analogies to heat transfer processes. *Measurements in Heat Transfer* (E. R. G. Eckert and R. J. Goldstein, Eds.), Hemisphere, Washington, DC, 397–423

Garcia, A. and Sparrow, E. M. 1987. Turbulent heat transfer downstream of a contraction-related, forward-facing step in a duct. *ASME J. Heat Transfer* **109**, 621–626

Good, M. C. and Joubert, P. N. 1968. The form drag of two-dimensional bluff plates immersed in turbulent boundary layers. *J. Fluid Mech.* **31**, 547–582

Incropera, F. P., Kerby, J. S., Moffat, D. F. and Ramadhyani, S. 1986. Convection heat transfer from discrete heat sources in a rectangular channel. *Int. J. Heat Mass Transfer* **29**, 1051–1058

Jones, Jr, O. C. 1976. An improvement in calculation of turbulent friction in rectangular ducts. *J. Fluids Eng.* **98**, 173–180

Kelkar, K. M. and Patankar, S. V. 1987. Numerical prediction of flow and heat transfer in a parallel plate channel with staggered fins. *ASME J. Heat Transfer* **109**, 25–30

Kline, S. J. 1985. The purposes of uncertainty analysis. *J. Fluids Eng.* **107**, 153–160

Krall, K. M. and Sparrow, E. M. 1966. Turbulent heat transfer in the separated, reattached, and redevelopment regions of a circular tube. *ASME J. Heat Transfer* **88**, 131–136

Mills, A. F. 1962. Experimental investigation of turbulent heat transfer in the entrance region of a circular conduit. *Journal of Mechanical Engineering Science* **4**, 63–77

Molki, M., Astill, K. N. and Leal, E. 1990. Convective heat-mass transfer in the entrance region of a concentric annulus having a rotating inner cylinder. *Int. J. Heat Fluid Flow* **11**, 120–128

Molki, M. and Mostoufizadeh, A. R. 1989. Turbulent heat transfer in rectangular ducts with repeated-baffle blockages. *Int. J. Heat Mass Transfer* **32**, 1491–1499

Perry, R. H. and Green, D. 1987. *Perry's Chemical Engineers' Handbook*, 6th ed. McGraw-Hill, Singapore, 3–39

Sogin, H. H. 1958. Sublimation from disks to air streams flowing normal to their surfaces. *ASME Transactions* **80**, 61–71

Sparrow, E. M. and Comb, J. W. 1983. Effect of interwall spacing and fluid flow inlet conditions on a corrugated-wall heat exchanger. *Int. J. Heat Mass Transfer* **26**, 993–1005

Sparrow, E. M., Garcia, A. and Chuck, W. 1987. Turbulent duct flow with streamwise nonuniform heating at the duct wall. *Int. J. Heat Mass Transfer* **30**, 175–185

Sparrow, E. M. and Wachtler, K. P. 1978. Transfer coefficients on the surfaces of a transverse plate situated in a duct flow. *Int. J. Heat Mass Transfer* **21**, 761–767

Vogel, J. C. and Eaton, J. K. 1985. Combined heat transfer and fluid dynamic measurements downstream of a backward-facing step. *ASME J. Heat Transfer* **107**, 922–929

Webb, B. W. and Ramadhyani, S. 1985. Conjugate heat transfer with staggered ribs. *Int. J. Heat Mass Transfer* **28**, 1679–1687